Computers in Biology and Medicine 110 (2019) 254–264

Contents lists available at ScienceDirect

Computers in Biology and Medicine

journal homepage: www.elsevier.com/locate/compbiomed

Decoding electroencephalographic signals for direction in brain-computer interface using echo state network and Gaussian readouts

Hoon-Hee Kim[a], Jaeseung Jeong[a,b,*]

[a] Department of Bio and Brain Engineering, College of Engineering, Korea Advanced Institute of Science and Technology (KAIST), Daejeon, 34141, Republic of Korea
[b] Program of Brain and Cognitive Engineering, Korea Advanced Institute of Science and Technology (KAIST), Daejeon, 34141, Republic of Korea

ARTICLE INFO

Keywords:
Brain-computer interface
Electroencephalography
Echo state network
Gaussian readout
Decoding movement direction

ABSTRACT

Background: Noninvasive brain-computer interfaces (BCI) for movement control via an electroencephalogram (EEG) have been extensively investigated. However, most previous studies decoded user intention for movement directions based on sensorimotor rhythms during motor imagery. BCI systems based on mapping imagery movement of body parts (e.g., left or right hands) to movement directions (left or right directional movement of a machine or cursor) are less intuitive and less convenient due to the complex training procedures. Thus, direct decoding methods for detecting user intention about movement directions are urgently needed.
Methods: Here, we describe a novel direct decoding method for user intention about the movement directions using the echo state network and Gaussian readouts. Importantly parameters in the network were optimized using the genetic algorithm method to achieve better decoding performance. We tested the decoding performance of this method with four healthy subjects and an inexpensive wireless EEG system containing 14 channels and then compared the performance outcome with that of a conventional machine learning method.
Results: We showed that this decoding method successfully classified eight directions of intended movement (approximately 95% of an accuracy).
Conclusions: We suggest that the echo state network and Gaussian readouts can be a useful decoding method to directly read user intention of movement directions even using an inexpensive and portable EEG system.

1. Introduction

Advancements in neuroimaging techniques including the electroencephalography (EEG), electrocorticography (ECoG), magnetoencephalography (MEG), and functional magnetic resonance imaging (fMRI) have led to the emergence of mind reading and the brain-computer interface (BCI) [1]. The BCI is a direct communication methodology between the brain and machines based on detection of neural activities [2]. This technology enables the control of computers or machines via human thought [3] as well as machines that respond to the emotional states of individuals [4].

Most BCI studies have used noninvasive decoders via EEGs; this approach is less expensive and more appropriate for healthy individuals [5,6]. EEG-based BCI techniques have successfully been used for the control of cursors [7–9], robotic arms [10–12], humanoid robots [13,14], and drones [15,16]. They have decoded the emotional states of individuals to control robotic systems and suitably respond to them [4,17–19].

For instance, remarkable studies by Wolpaw and colleagues have successfully translated sensorimotor rhythms obtained from conventional 64-channel EEG recording systems and applied them to two- [7] and three-dimensional [8] cursor movements on a computer screen using adaptive algorithms and a large Laplacian filter. LeFleur et al. proposed BCI control systems for drones in three-dimensional space using motor imagery signals and 64-channel EEG systems [15]. In addition, we have successfully demonstrated more practical BCI control systems for humanoid robots in two-dimensional space using motor imagery signals and 32-channel EEG systems [13]. While these BCI systems have been developed based on classifications of sensorimotor rhythms during a motor imagery task [20–22], other BCI systems have focused on predicting the motion trajectory [3,11] or recognizing the user's cognitive states [4,17,23–25]. For example, Kim et al. used inexpensive 16-channel EEGs with the hybrid BCI/eye-tracker system to classify the attention levels of BCI users to control a drone in three-dimensional space [16].

However, it is quite difficult to decode the intention of the BCI users

* Corresponding author. Department of Bio and Brain Engineering, Korea Advanced Institute of Science and Technology (KAIST), 291 Daehak-ro, Yuseong-gu, Daejeon, 34141, Republic of Korea
E-mail addresses: jsjeong@kaist.ac.kr, jsjeong@complex.korea.ac.kr (J. Jeong).

https://doi.org/10.1016/j.compbiomed.2019.05.024
Received 2 April 2019; Received in revised form 31 May 2019; Accepted 31 May 2019

using the EEG because the EEG has lower spatial resolutions and less information content due to involvement of a large size of neuronal populations relative to neuroimaging tools [26–28]. Thus, most previous BCI studies have utilized well-defined electrical signals of the brain such as event-related potentials or motor imagery signals [29]. For example, brain signals elicited during the motor imagery of the left or right hand are used as a command signal for “move to the left” or “move to the right” for the robotic drone, respectively. Signals for the motor imagery of both hands can be used as a “move forward” command similar to the signals from joysticks to induce movement. In essence, these methods monitor the sensorimotor rhythms from the motor cortex and compare their power spectra between left and right regions of the brain during the performance of a motor imagery task [27].

In addition, conventional EEG recording systems are too large and heavy, and utilize particularly uncomfortable protocols involving wet electrodes. Recently, less-expensive and portable EEG systems such as OpenBCI, EMOTIV, and NeuroSky have become available, but they have lower sampling rates, worse signal-to-noise ratios, and fewer channels than conventional EEG recording systems. This impedes their ability to decode the sensorimotor rhythms and thus the intention of the BCI user.

Therefore, the aim of this study was to develop a novel EEG decoder for BCI applications of movement control that can classify the user intention of movement directions using an inexpensive EEG recording system. In this study, we investigated the potential usefulness of the echo state network. The echo state network analyzes and predicts nonlinear time series yet has very simple learning rules for readouts [30]. Here, we used the readouts with Gaussian properties to represent movement directions. An EMOTIV EPOC + system was used as a portable and inexpensive EEG recording system to record EEG signals in 14 channels to directly read subjects’ intention of movement directions rather than imagery movement of their bodies.

2. Methods

2.1. Subjects

Four male individuals participated in this study. Subjects A and B were 20 years old, subject C was 21 years old, and subject D was 23 years old. The aim of this study was to design and test an EEG decoder for healthy BCI users, and patients with paralysis or epilepsy were not utilized. All participants were right-handed and had normal or corrected to normal vision with no history of neurological or psychiatric abnormalities. None of the subjects had prior experience with BCI or EEG. The subjects were informed of the experimental protocols and study objective prior to participating, and all consented to participation. The Institutional Review Board (IRB) of KAIST approved the proposed experimental protocol of this study.

2.2. EEG recording

An EMOTIV EPOC + system was used to record wireless EEG signals via Bluetooth with semi-dry electrode sensors (saline-soaked felt pads) and a comfortable headset for daily use or in any situation. The EPOC + system includes 14 channels (AF3, F7, F3, FC5, T7, P7, O1, O2, P8, T8, FC6, F4, F8, and AF4) plus two (Common Mode Sense (CMS) active electrode and Driven Right Leg (DRL) passive electrode) for references that record at a sampling rate of 128 Hz (Fig. 1). This system has a lower specification than conventional EEG systems such as the Compumedics Neuroscan system which usually provides 32-256 wet channels and high sampling rates of 256 - 20,000 Hz [13].

2.3. Experimental stimuli

To mimic the subject's vision during movement, stimulus animations were made of a grid moving in eight different directions (Fig. 2a);

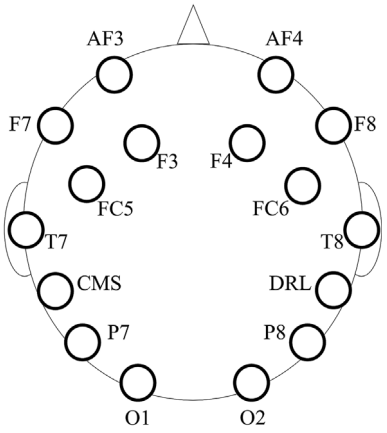

Fig. 1. Electrode positions of the EMOTIV EPOC+. EMOTIV EPOC + had 14 channels for EEG recording (AF3, F7, F3, FC5, T7, P7, O1, O2, P8, T8, FC6, F4, F8, and AF4) and two channels for references (CMS and DRL) with a sampling rate at 128 Hz.

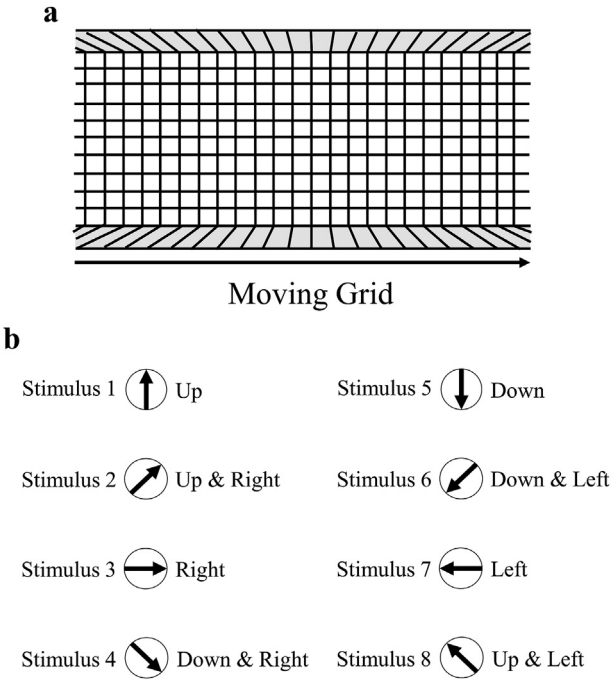

Fig. 2. Stimulus descriptions. (a) Example of a grid stimulus with the direction of movement indicated at the bottom (stimulus 3). The stimuli were designed to mimic the subject's point of view during movement. (b) Eight stimuli representing different directions were used.

stimulus 1 was movement in an upward direction, stimulus 2 was movement upward and to the right, etc. (Fig. 2b). The stimuli thus guided the subjects to think about moving in a specific direction. To remove the effect of motor imagery, the subjects were instructed to intend to directly move only in a certain direction rather than think about moving a body part when the stimulus was given.

2.4. Experimental protocol

The subjects followed on-screen instructions during EEG recording. A trial began when a cross dot appeared at the center of the screen (Fig. 3). After 10 s (resting period), the moving grid stimulus was displayed for 5 s followed by a “stop” screen for 30 s. The subjects were instructed to keep thinking about moving in the direction indicated by the preceding stimulus. The direction of the stimulus was then

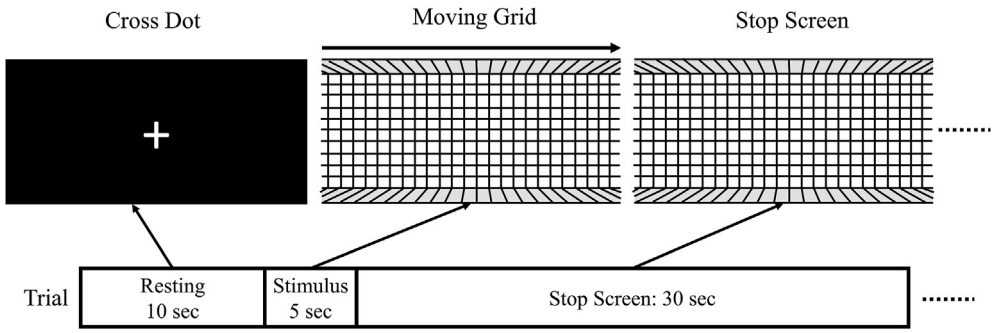

Fig. 3. Experimental protocol. A cross dot was displayed at the center of the screen for 10 s (resting period). Then, a moving grid animation (stimulus) was played for 5 s followed by a stationary grid (stop screen) for 30 s during which the subject was instructed to keep thinking about the direction of movement.

randomly selected in a uniform distribution; therefore, the order of the eight stimuli differed among trials—each of which lasted 6 min. The EEGs were recorded for the entire duration of the experiment, but only the signals for the "stop screen" period and the "resting" period were used to train and test the decoder. A single session consisted of 10 trials with 1 min between each trial. The subjects underwent three sessions per week for training and testing for a total of 11 sessions for subject A, 10 sessions for subject B, and 12 sessions each for subjects C and D.

2.5. Preprocessing

Numerous artifacts are also captured when measuring EEG signals. In particular, artifacts with amplitudes higher than the brain-related signals cause difficulty when analyzing EEG signals. Typical artifacts affecting EEG include eye movements, muscle contractions, and line noise artifacts. Many EEG studies have successfully applied independent component analysis (ICA) algorithms to remove artifacts [31,32]. ICA algorithms decompose the raw neural signals into independent components, find artifact components via pattern and source localization analyses, and subtract the artifact components from the raw neural signals thus creating brain-related signals without artifact components. However, most means of determining components related to artifacts largely depend on user-selected components. We used the ICA-based algorithm ADJUST to remove artifacts precisely [33]; this algorithm automatically determines artifact-related components. ADJUST uses specific spatial and temporal features of stereotype artifacts (e.g., eye blinking, muscle movements) to determine independent components of artifacts automatically. We subtracted these components from the raw data and thus cleaned the EEG data for the decoder.

We also applied filtering and a spectral analysis to the EEGs. First, a 1–64 Hz band-pass filter and a 55–65 Hz notch filter were applied to remove 60 Hz line noise. Second, the filtered EEG data underwent an autoregressive spectral analysis [34]. The model order of the autoregressive spectral analysis was fixed at 16 according to a previous study [35]. To extract the features of the EEGs, every 300 msec observation segment recorded for 3 s from fourteen channels was analyzed with an autoregressive algorithm. The square root of the power in 2-Hz-wide frequency bands within 1–64 Hz and significant brain-wave frequency bands were calculated. Here, these bands were the delta (1–3 Hz), theta (3–8 Hz), alpha (8–12 Hz), beta (12–38 Hz), and gamma (38–42 Hz) frequencies. In total, 37 feature vectors with 518 dimensions (14 channels × 37 frequency components in the 1-64 Hz band with 2 Hz bins and specific frequency components, i.e., the delta, theta, alpha, beta, and gamma components) were collected within the 'stop screen' periods (30 s × 8 directions) and rest periods (10 s × 8 times) for one trial.

All input features were linearly normalized according to the following equation:

$$\bar{u} = 2 \times \frac{u - m}{M - m} - 1,$$

Here, u is the original value of the input features, m is the minimum value of the input features, and M is the maximum value of the input features.

2.6. Echo state network

The echo state network was first proposed by Jaeger and Haas [30]— a recurrent neural network with a sparsely connected internal unit (hidden) layer (Fig. 4). This recurrent neural network was designed particularly for non-linear time series prediction and complex system analysis.

The weights of neurons in the internal unit layer were fixed and have sparse random connectivity. The weights of neurons in the output (readout) layer could be learned so that the network could produce specific temporal patterns. Unlike conventional recurrent neural networks, the echo state network had a fading or short-term memory. The current state of the neurons in the internal unit layer, called the echo state, was affected by continuous input streams. Thus, the most recent input information had the greatest impact on the echo state network, and its influence decays over time [36].

Another feature of the echo state network was that it had a recurrent network structure but simpler learning methods than a conventional recurrent neural network. The input layer linearly connected to the internal units and the readout layer. The internal units had recursive connections and also linearly connected to the readout layers. Readout units received data linearly from the internal unit layers; connections between readouts were also allowed. Thus, all readouts of the echo

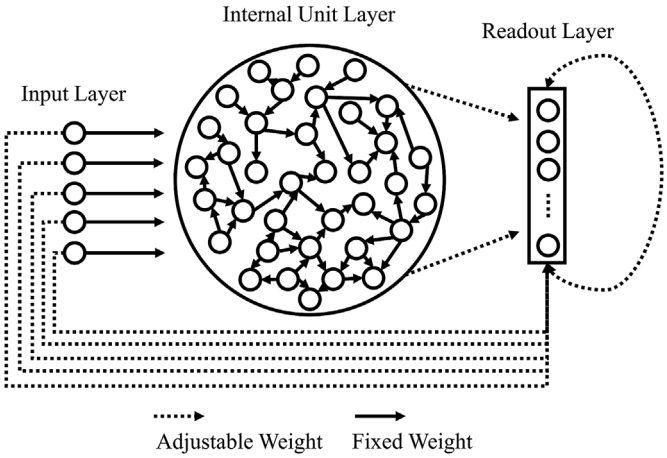

Fig. 4. Structure of the echo state network. The echo state network consisted of three layers: input layer, the internal unit layer, and the readout (output unit) layer. Units of the input layer were connected with fixed weights to the internal units that had recursive connections with fixed weights. The readouts were linearly connected from the input and internal layers with adjustable weights; connections between readouts were allowed.

state network were linearly connected from each layer. The echo state network worked with any simple linear learning rules because the weights of the input and internal units were randomly selected and fixed when the network was initialized and only the weights of readouts were adjusted during training sessions. Although the learning rule of the echo state network was simple, the echo state network could solve complex problems. The echo state network had a sufficient number of internal units to expand the information from inputs to a higher dimension when there was sufficient problem-solving space to produce the best solution [37–39]. Thus, echo state networks have been used in the analyses of EEG signals [18,19,40,41] and brain modeling [42,43] as well as various engineering fields [44–47].

For the standard echo state network, $u(t+1)$ was an input vector at time step $t+1$. The state of the internal unit was expressed as the following equation:

$$x(t+1) = f(W^{\text{in}} \cdot u(t+1) + W \cdot x(t) + W^{\text{back}} \cdot y(t)),$$

where f is the activation function of the internal units (such as the sigmoid function) and W^{in}, W, and W^{back} were weight matrices of input to internal, internal to internal, and readout to internal layers, respectively. The units of the output layer (i.e., readouts) were updated according to the following equation:

$$y(t+1) = W^{\text{out}} \cdot (u(t+1), x(t+1), y(t)),$$

where $(u(t+1), x(t+1), y(t))$ is the concatenation of input units, internal units, and previous readouts vectors, respectively. The main characteristic of the echo state network was that it is only tuned by W^{out} for any supervised linear learning rule. In this study, the Moore-Penrose inverses of the matrices were used [48,49].

The echo state network in this study was initialized with N internal units with 1% interconnectivity, and all weights were randomly sampled from a uniform distribution between -1 and 1. The weight matrix of internal units was rescaled so that the magnitude of the largest eigenvalue of the internal weight matrix, $|\lambda_{\max}|$, was < 1. This was because of the spectral radius of the internal weight matrix effect to the performance of the echo state network [37,38].

2.7. Readout design

The performance of the echo state network was dependent on how the readout (the output of the network) was designed. Thus, a Gaussian property was used for the readout to create direction preferences according to the following equation:

$$f_n^{\text{out}}(\theta) = \frac{1}{(2\pi\sigma^2)^{\frac{1}{2}}} \exp\left\{-\frac{1}{2\sigma^2}(\theta - \theta_n)^2\right\} = W_n^{\text{out}} \cdot (u_\theta(t+1), x(t+1), y(t)),$$

Here, f_n^{out} denotes the Gaussian activation function of the readouts with preference for the specific direction θ_n, θ is the direction of the stimulus, u_θ is the input feature vector of the θ direction stimulus, n is the index of the readouts, and σ is a parameter of readout functions that controls the width of the readout tuning curve. Fig. 5 shows an example of a typical design of readout units. The response of the readout was the highest when the preferred direction was given as a stimulus. The response of the readout decreased in a Gaussian fashion as the angle from the preferred direction changed.

Every readout had a different W^{out} to have a preference for a specific direction. For example, the weight vector W_1^{out} of readout 1 was tuned to f_1^{out} to have a maximum response when the given stimulus was θ_1. This indicates the direction UP. The weight vector W_2^{out} of readout 2 was tuned to f_2^{out} to provide a maximum response when the given stimulus was θ_2 indicating directions UP and RIGHT. The input feature vector u_θ depended on the stimulus direction θ. In addition, every readout was tuned to a zero response when the given stimulus is "resting."

2.8. Parameter optimization

The performance of the echo state network is known to be largely affected by the size of the internal units (N) [37], the spectral radius of the internal weight matrix (λ),the network connectivity [38], and nonlinearity [39]. The optimal values of these parameters were task-specific. In this study, three parameters (N, λ, and the readout parameter σ) were optimized using a genetic algorithm.

The goal of this optimization process was to minimize the difference between $f_i^{\text{target}}(\dot{\theta})$ and $f_i^{\text{out}}(\dot{\theta})$; thus, the fitness function of the genetic algorithm was defined as follows:

$$\text{fitness}(\dot{\theta}) = \sum_{i=1}^{n} f_i^{\text{target}}(\dot{\theta}) - f_i^{\text{out}}(\dot{\theta}),$$

where i is the index of the readout, $\dot{\theta}$ is the direction of the input stimulus, and $f_i^{\text{target}}(\dot{\theta})$ and $f_i^{\text{out}}(\dot{\theta})$ are the target value of readout i and the actual value of readout i when the given direction of stimulus is $\dot{\theta}$. The target value $f_i^{\text{target}}(\dot{\theta})$ followed a Gaussian tuning curve that was used to design the readout. Therefore, the final total fitness function for all stimuli was

$$\text{Total fitness} = \sum_{j=1}^{m} |\text{fitness}(\dot{\theta}_j)|,$$

where j is the index of the stimulus.

A genetic algorithm was used to find the optimal parameter values that minimized the value of the total fitness. This algorithm had four steps: initialization, selection, crossover, and mutation. In the initialization step, the three parameters N, λ, and σ (the genetic chromosomes) were randomly selected and distributed in the solution domain ([5,000, 100,000], [0, 1], and [0, 1], respectively); the fitness values of these chromosomes were calculated as potential solutions of problems. In the selection step, the genetic algorithms selected the best chromosomes for minimum fitness values and preserved them for the next generations. In the crossover step, the parameters of these chromosomes were exchanged to make new offspring. Genetic algorithms were subject to the local minima of the solution space, and thus a few of the selected parameters and exchanged chromosomes were subsequently mutated depending on a low probability. The genetic algorithm evaluated the new fitness values of the remaining chromosomes, and the last three steps were repeated until the remaining chromosomes and fitness values converged.

As an example of the parameter optimization process, the genetic algorithm created ESN decoders using the initially distributed chromosomes (N, λ, and σ) once a training set and a test set were given. It then evaluated the fitness values of each readout of the ESN decoders. Genetic algorithms selected chromosomes with the best fitness values and preserved them for the subsequent generations. The selected chromosomes made the next generation by exchanging and mutating. With the new generation of chromosomes, the genetic algorithm can then again create new ESN decoders to evaluate their fitness values. These processes were repeated until the remaining chromosomes and the fitness values converged.

3. Results

3.1. Temporal response of the decoder

The workflow diagram of our decoder is depicted in Fig. 6 for investigations of the temporal responses of the decoder layers. The decoder had 518 input streams (14 channels x 37 spectral power series [1–64 Hz with 2 Hz bins, delta, theta, alpha, beta, and gamma frequencies]). These channels were continuously and linearly processed in the internal units and modified via their recurrent connections. The weights of the internal units were fixed when the decoder was initialized. The input datum streams and the internal unit responses were

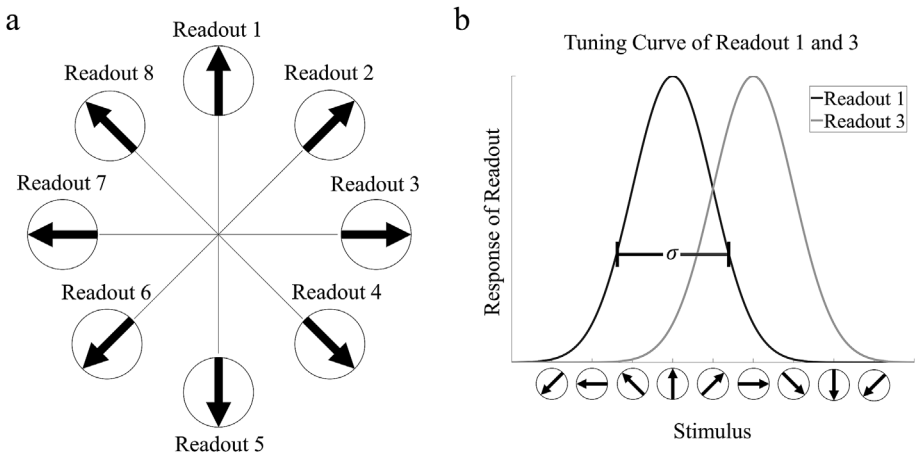

Fig. 5. Examples of readout design. (a) Eight readouts were constructed—each with a different direction preference. (b) Tuning curve for readout 2; the highest value for this readout occurred when the input stimulus was in the up and right direction. The response was reduced when the direction of the input stimulus differs from the preferred direction according to a Gaussian function and parameter σ; these affected the tuning width of the readout curve.

the inputs for each readout. Readout weights were linearly connected and adjusted such that they had a Gaussian tuning curve for the preferred direction. The temporal responses of the readouts changed according to the direction of the stimulus. All units in the decoder responded in real time to the input datum streams.

3.2. Readouts

A ten-fold cross-validation method was used to evaluate the performance of the decoder. Fig. 7 shows the training and test datasets for each session. Each session consists of ten trials: Nine trials were used for the training dataset, and one trial was the test dataset. Each trial consists of EEGs of eight directions with a resting period. The performance of the decoder averaged the results of each fold and session. All subjects had a different number of sessions (Subject A:11, Subject B: 10, Subject C: 12, Subject D: 12). The test sessions had 10-sec resting periods before the direction of the stimulus was given. The order of the directions of the stimulus was randomly selected in each case. Fig. 8 show temporal response of each readout in test sessions. Every readout immediately responded to the input signals and showed a different temporal response depending on the preferred direction.

We calculated the average readout responses for each stimulus over time to examine the performance of the decoder in classifying the different directions of the stimuli. We found that the response of the readout was highest when the given stimulus corresponded to the preferred direction of the readout and gradually decreased when the stimulus deviated from the preferred direction according to a Gaussian distribution. Fig. 9 shows the average responses for each of the readouts from various stimuli with a 10-fold cross-validation. Every readout for the four subjects clearly showed a direction preference that classified the stimulus direction. The highest response for the readout occurred when the stimulus for the preferred direction was given.

The decoder determined the direction of the stimulus using a winner-take-all method in every 300 msec. The decoder found the readout that had the highest response value for the given stimulus. This determined the preferred direction of readout as the final output of the decoder. Table 1 shows the classification performance (hit rate) of the decoder for each subject. These results show that the decoders have an

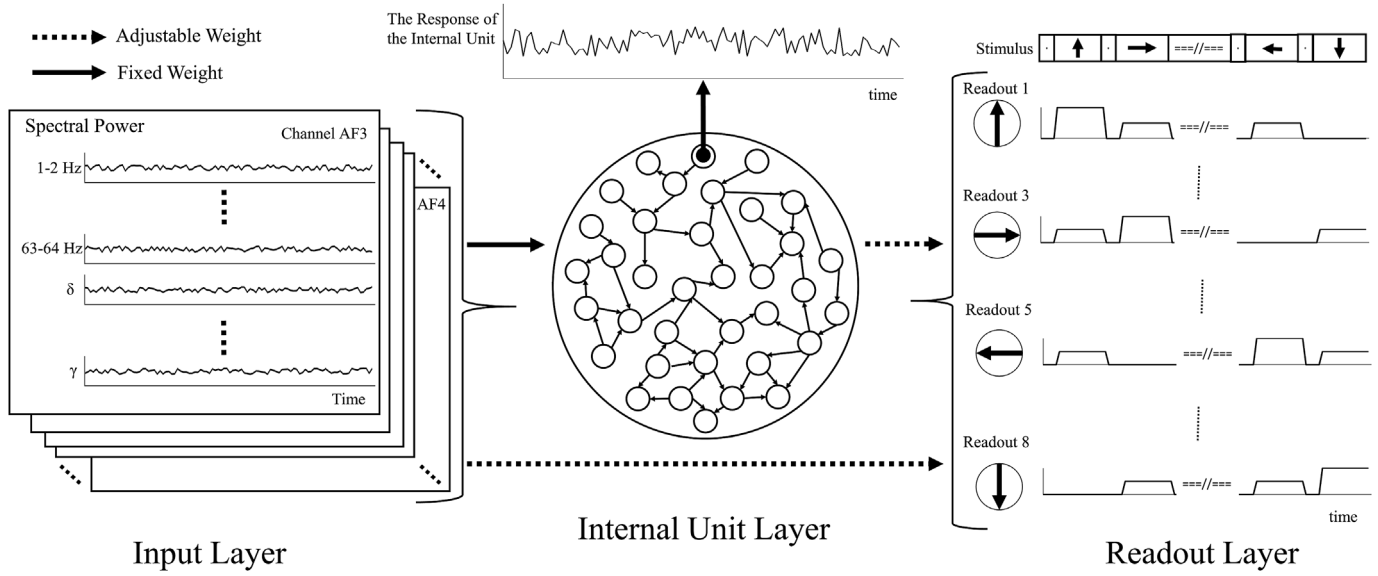

Fig. 6. Schematic examples of the decoder response. (Left) The input layer depended on the direction of the stimulus; the input streams were projected to the internal units. The input streams consisted of 37 features (spectral power of 1–64 Hz with 2 Hz bins, delta, theta, alpha, beta, and gamma frequencies) for each EEG channel. The weight of the input layer to the internal layer was fixed when the decoder was initialized, but the weight of the input layer to the readout layer was adjusted by the learning rule of the decoder. (Middle) The response of the internal layers was affected by the input datum streams and by recurrent connections between the internal units. All weights of internal units were fixed. (Right) The weights of the readouts were tuned for the readout layer to have a preference for a particular direction. Therefore, the response of the readouts depended on the direction of the stimulus and had the highest value when the preferred stimulus was given. The top of the readout plot shows the direction of stimulus or resting step as a function of time.

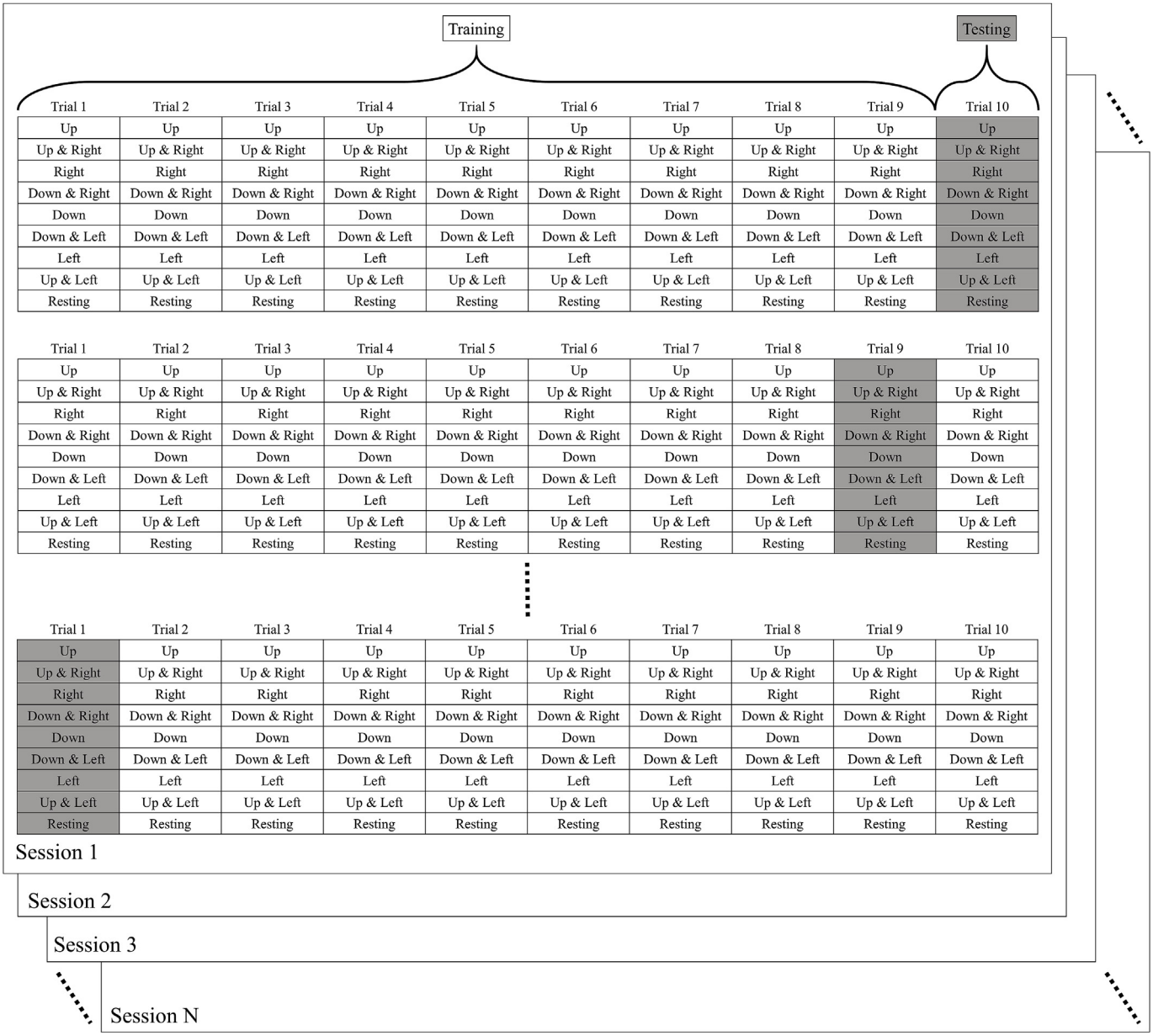

Fig. 7. Description of the ten-fold cross-validation dataset. One trial (shaded box) was used for the test dataset and the remaining trials (clear box) were used for training dataset. Each trial consists of eight directions and a rest period. The number of sessions depends on the subject (Subject A: 11, Subject B: 10, Subject C: 12, Subject D: 12).

average classification performance of 98.3% over all stimuli and subjects. These results also demonstrate that the proposed decoder can precisely classify eight directions of the stimulus.

3.3. Reduced number of readouts

We next investigated the possibility of reducing the number of readouts from eight to four using the Gaussian property of the readouts and a proper threshold. We hypothesized that if readouts 1, 3, 5, and 7 were well tuned to have Gaussian properties, then the decoder could reduce readouts 2, 4, 6 and 8 using an appropriate threshold. When the given direction of the stimulus is UP & RIGHT (preferred direction of Readout 2), it can decode the direction under certain conditions such that the responses of Readouts 1 and 3 are higher than the threshold, and the responses of Readout 5 and 7 are lower than the threshold (Fig. 10). The decoder can determine that the input stimulus is the preferred direction of the readout when only one readout response is higher than the threshold. Based on this hypothesis, we can eliminate readouts 2, 4, 6, and 8 and retain readouts 1, 3, 5, and 7 such that readout 2 was replaced by readout 1 or 3; readout 4 was replaced by readout 3 or 5, etc. Fig. 11 shows the responses for readouts 1, 3, 5, and 7 over 80 trials (80 trials = ten-fold cross-validation; each fold has eight directions; see Fig. 7).

To evaluate the performance of the decoder using the reduced number of readouts, we counted the number of errors (i.e., when the decoder decided the wrong stimulus class) and calculated the hit rate of the decoder. We found that the classification performance for the reduced number of readouts depended on the threshold (Fig. 12). The best classification performance (approximately 95% of hit rate) was achieved using the reduced number of readouts at a certain threshold.

3.4. Classification performance of a conventional machine learning method

We next measured the performance of the decoder with that of a

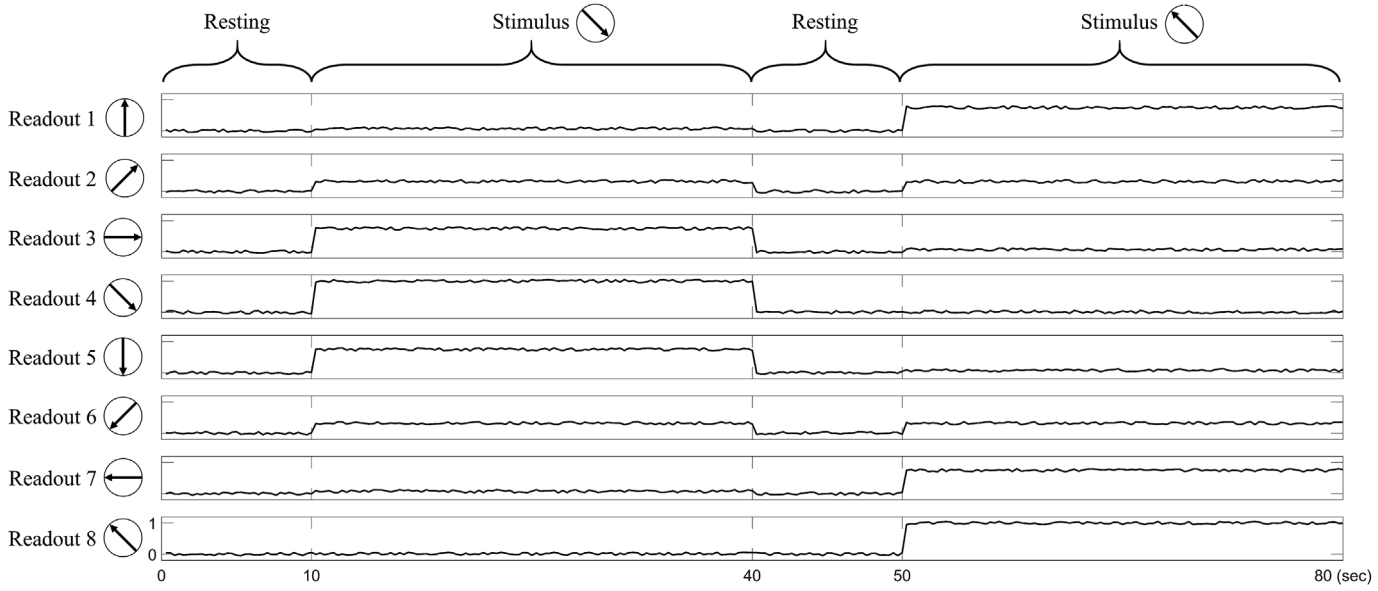

Fig. 8. Temporal response of the readouts. Each readout shows a different temporal response depending on the preferred direction. The given stimuli followed the sequence order of 10 s for resting, 30 s for DOWN & RIGHT, 10 s for resting, and 30 s for UP & LEFT.

conventional learning machine method—the support vector machine (SVM). The objective of this analysis was to measure the difficulty of classification directions with our experimental environment. Our decoder perfectly classified eight directions (Fig. 9 and Table 1), and thus we initially examined whether the SVM decoder can classifies the right and left directions with low classification difficulty before considering all eight directions.

We used nonlinear SVM with polynomial kernels and EEG features (spectral power series in a 2-Hz-wide frequency band within 1–64 Hz and delta (1–3 Hz), theta (3–8 Hz), alpha (8–12 Hz), beta (12–38 Hz), and gamma (38–42 Hz) frequencies with 3000 msec segmentations and 300 msec sliding lengths. This step used the purposed decoder but only considered the dataset for the left and right directions. The SVM decoder was supervised and taught to classify the left or right direction via input features meaning that the SVM decoder classified a direction

Table 1
Classification performance (hit rate) of the decoder.

	Stimulus 1	Stimulus 2	Stimulus 3	Stimulus 4
Subject A	100.0 ± 0.0	97.3 ± 2.6	100.0 ± 0.0	99.5 ± 0.5
Subject B	94.9 ± 5.1	100.0 ± 0.0	97.0 ± 2.9	95.6 ± 3.4
Subject C	99.6 ± 0.4	100.0 ± 0.0	98.0 ± 1.7	99.7 ± 0.2
Subject D	93.5 ± 5.1	100.0 ± 0.0	94.2 ± 3.6	98.5 ± 1.5
	Stimulus 5	Stimulus 6	Stimulus 7	Stimulus 8
Subject A	95.0 ± 3.3	94.2 ± 4.0	99.8 ± 0.2	100.0 ± 0.0
Subject B	100.0 ± 0.0	100.0 ± 0.0	98.8 ± 1.2	98.5 ± 1.4
Subject C	95.9 ± 3.1	100.0 ± 0.0	100.0 ± 0.0	94.3 ± 4.2
Subject D	98.5 ± 0.9	100.0 ± 0.0	95.9 ± 2.4	98.4 ± 1.4

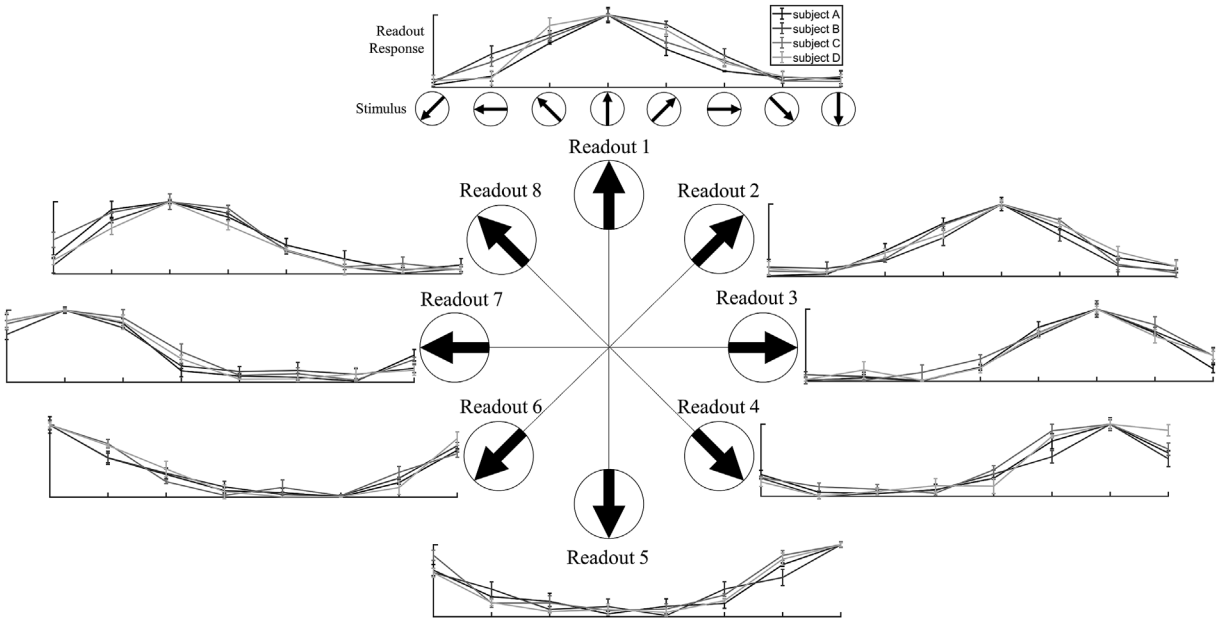

Fig. 9. Readouts for subjects A, B, C, and D. The decoder had eight readouts, and each had a directional preference. Each plot shows the average responses (y axis) for the readout for the various stimuli along the x axis. These results were obtained using a 10-fold cross-validation.

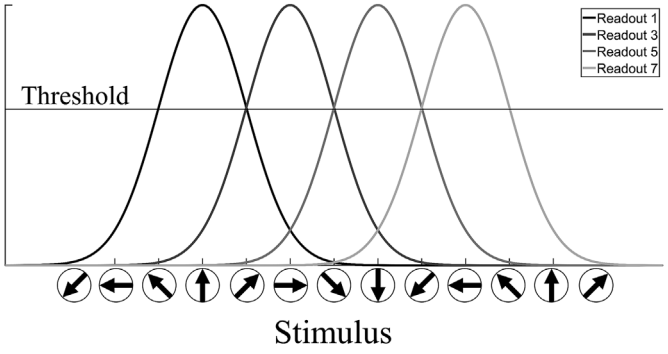

Fig. 10. Design of the reduced readouts with a threshold. Readouts 1, 3, 5, and 7 can alternatively represent readouts 2, 4, 6, and 8. For example, when the responses of readouts 1 and 3 exceeded the threshold—and the responses of readouts 5 and 7 were lower than the threshold—the decoder can determine that the given direction of the stimulus is UP & RIGHT.

every 300 msec in one trial. The performance was averaged in terms of the hit rate for every classified result.

The SVM was strongly influenced by the feature selection, and thus we not only considered all EEG channels but also evaluated the performance by selecting the channels corresponding to the left and right hemispheres of the brain as the features. This approach was previously used to study classifications of left and right directions in BCI in conventional EEG systems [7,13,15]. For example, the SVM decoder classified left and right directions using EEG data from the F3 channel located on the left hemisphere and EEG data from the F4 channel located on the right hemisphere.

The performance measured the average hit rate of the SVM decoder with a ten-fold cross-validation for each session (Fig. 13). The best hit rate performance for the classification of left and right directions with the SVM decoder was approximately 50% (Table 2) in our experimental environment via an inexpensive EEG system. This result indicates that the SVM decoder can only classify directions at the chance level over two direction classification tasks. However, the proposed decoder outperformed the SVM decoder because it could classify the directions precisely over eight directions (see Fig. 9).

4. Discussion

We report a decoder utilizing an echo state network and Gaussian readouts that successfully classified the movement directions from EEG signals. Rather than relying on motor imagery in which the sensorimotor rhythms of the motor cortex are akin to a joystick to induce the directional movement of body parts [7,8,13,15], the proposed method utilizes EEG signals that are directly associated with the user's intention—this approach is more natural, intuitive, and convenient for BCI applications.

Our proposed decoder has eight readouts to represent different directions. The directional preference for each readout has a Gaussian distribution such that the highest response value corresponds to the preferred direction (Fig. 9 and Table 1). This enables us to reduce the number of readouts to four with an appropriate threshold for the response values. Decreasing the number of readouts reduces the amount of computation required in the decoder and can utilize an inexpensive

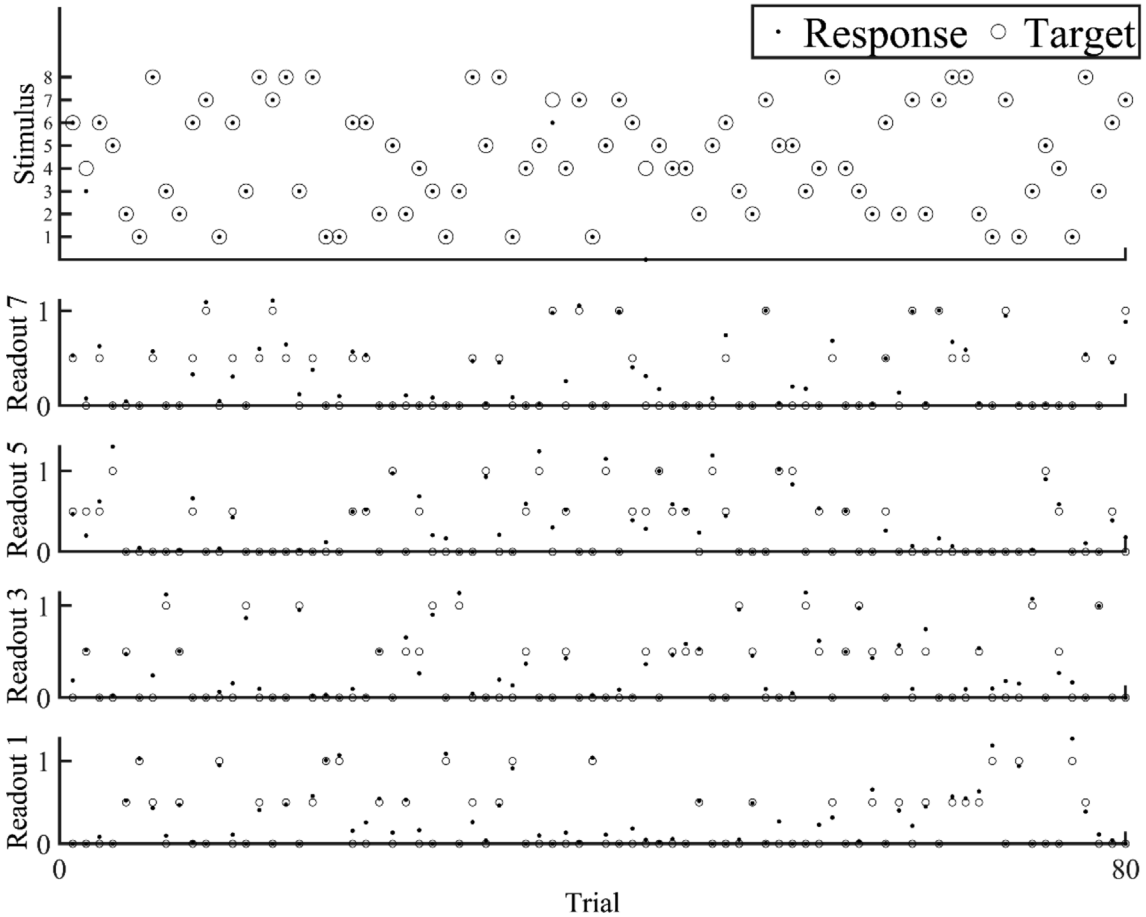

Fig. 11. Reduced number of readouts. Top plots show the differences between the classification of the target stimulus (circles) and the actual decisions/responses from the reduced readouts (dots) using a certain threshold. The bottom three plots show the differences between the target responses of the readouts (circles) and the actual responses of the readouts (dots). The decoder was tested ten times over eight directions for a total of 80 trials for each readout (*y* axis).

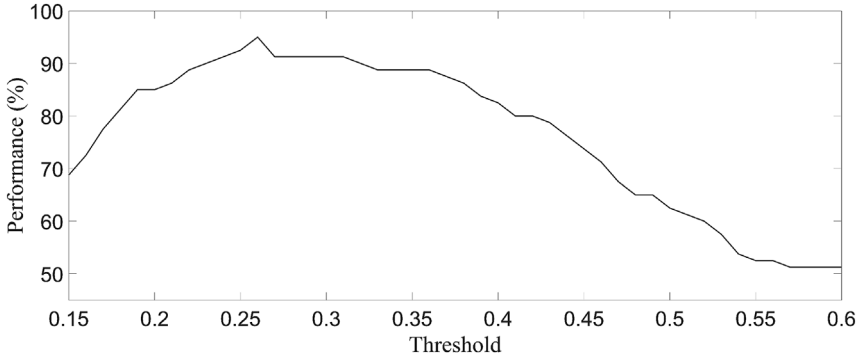

Fig. 12. Classification performance (hit rate) as the threshold value changed.

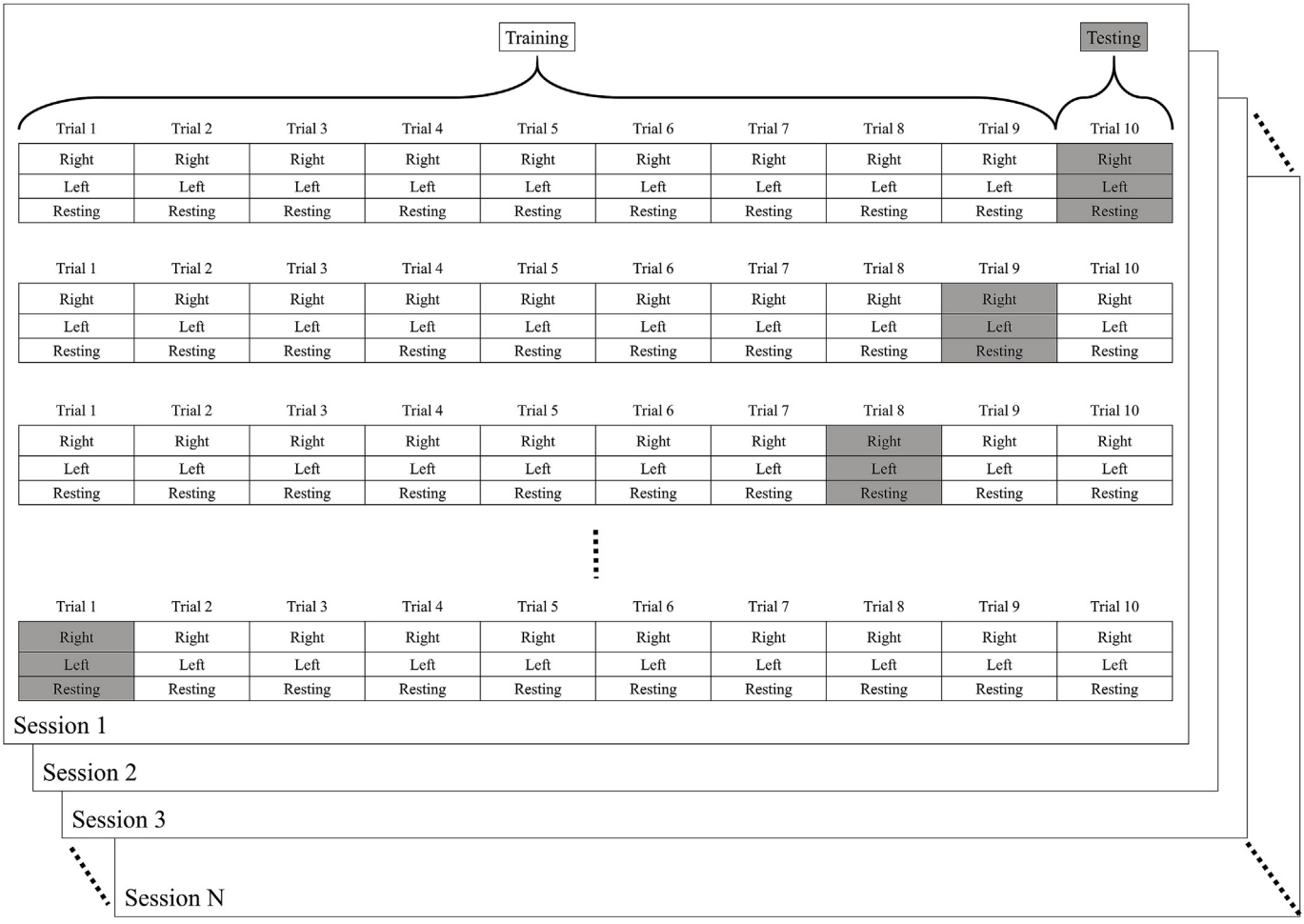

Fig. 13. Description of the ten-fold cross-validation dataset. One trial (shaded box) used the test dataset, and the remaining trials (clear box) used the training dataset. Each trial consisted of two directions and a resting period. The number of sessions depended on the subject (Subject A: 11, Subject B: 10, Subject C: 12, and Subject D: 12).

Table 2
Classification performance (left and right direction) of the SVM decoder using the EEGs obtained from an inexpensive EEG recording system.

Subject	Performance (%) for EEG channels:							
	All	AF3, AF4	F7, F8	F3, F4	FC5, FC6	T7, T8	P7, P8	O1, O2
A	49.1 ± 9.5	49.6 ± 15.3	56.9 ± 6.6	45.8 ± 11.5	45.0 ± 12.9	50.0 ± 16.8	50.0 ± 11.2	47.7 ± 11.1
B	48.2 ± 10.1	51.2 ± 5.1	26.5 ± 13.3	56.2 ± 9.6	51.9 ± 9.3	60.0 ± 10.5	60.0 ± 6.1	47.3 ± 18.8
C	49.4 ± 8.8	41.5 ± 13.3	48.5 ± 11.4	47.7 ± 11.7	52.3 ± 6.7	61.5 ± 14.1	58.1 ± 9.9	48.8 ± 10.0
D	52.9 ± 16.8	58.8 ± 20.2	38.1 ± 25.5	64.6 ± 9.2	58.0 ± 17.3	34.2 ± 27.8	57.3 ± 19.9	62.3 ± 13.6

EEG recording system. Here, the 95% hit rate was successfully achieved only when using four readouts, which is sufficient for many BCI applications. Because the proposed decoder also immediately responded to the input signals and precisely classified the directions (Fig. 8), it is appropriate for use in practical BCI environments such as those that rely on real-time processes.

One of the advantages of our decoder is that it produces high performance using an inexpensive and wireless EEG recording system with a small number (i.e., 14) of electrode channels and a low sampling rate (128 Hz) versus more expensive recording systems (sampling rates of > 1,000 Hz and > 32 electrode channels) [7,8,13,15]. Our decoder possibly extends the possibilities for inexpensive EEG recording systems into other applications of BCI or mind-reading including the classification of attention and inattention [16].

The echo state network utilizes a simple linear learning rule to project an input into a large number of internal units amplifying the problem-solving space [30]. For this reason, our proposed decoder does not require feature selection processes to classify the direction of intended movement from EEG signals. Nevertheless, the echo state network is somewhat of a black box for which the internal computations are difficult to identify and assess in detail.

Various parameters potentially influence the performance of the echo state networks; their values can vary according to the task. Here, we employed genetic algorithms to optimize such parameters (N, λ, and σ) for each session and subject; this approach increased the accuracy of the decoder but also the computational burden. Additional parameters may further improve the performance of the echo state network such as the structure of internal units, feature selection for preprocessing, and the learning rule for readouts—these should be investigated in the future.

The decoder proposed here successfully represented directions in a two-dimensional space: the horizontal and vertical axes using eight and even four readouts. Ideally, the two-dimensional space can represent two readouts as vector expression. The main problem of two readouts is likely that a task of the decoder would be regression rather than classification. During a classification task, the decoder has to determine a specific direction via the readout that has the highest response. In the case of regression however, the response of the two readouts must be a real number to specify the direction. Thus, the regression of the responses to only two readouts per axis renders subsequent analyses more difficult. Moreover, many BCI applications such as those involving robot or drone control are performed in three-dimensional space. The method described here pertains to directionality in two-dimensional space, and further studies on the activation function are required to attain readouts for three-dimensional space with this system.

Nevertheless, our proposed decoder successfully classifies EEG signals for the intended directional movement without motor imagery using an inexpensive and portable EEG recording system. This method potentially paves the way for further advancements in BCI applications in a variety of situations using more intuitive commands with user-friendly inexpensive EEG systems. We suggest that the echo state networks and well-designed readouts are useful for direct decoders in advanced BCI research.

Conflicts of interest

None Declared.

Funding

This study was supported by the Brain Research Program through the National Research Foundation of Korea (NRF) funded by the Ministry of Science, ICT and Future Planning [2016M3C7A1904988]; and This paper is based on a research which has been conducted as part of the KAIST-funded Global Singularity Research Program for 2019; This work was supported by Samsung Research Funding Center of Samsung Electronics under Project Number [SRFC-TC1603-06]; and This work was supported by Hyundai Motor Company.

References

[1] P.R. Roelfsema, D. Denys, P.C. Klink, Mind reading and writing: the future of neurotechnology, Trends Cognit. Sci. 22 (2018) 598–610.
[2] M.A. Lebedev, M.A. Nicolelis, Brain-machine interfaces: past, present and future, Trends Neurosci. 29 (2006) 536–546.
[3] H.G. Yeom, J.S. Kim, C.K. Chung, Estimation of the velocity and trajectory of three-dimensional reaching movements from non-invasive magnetoencephalography signals, J. Neural Eng. 10 (2013) 026006.
[4] D.J. McFarland, M.A. Parvaz, W.A. Sarnacki, R.Z. Goldstein, J.R. Wolpaw, Prediction of subjective ratings of emotional pictures by EEG features, J. Neural Eng. 14 (2017) 016009.
[5] F. Lopes da Silva, EEG and MEG: relevance to neuroscience, Neuron 80 (2013) 1112–1128.
[6] M.X. Cohen, Where does EEG come from and what does it mean? Trends Neurosci. 40 (2017) 208–218.
[7] J.R. Wolpaw, D.J. McFarland, Control of a two-dimensional movement signal by a noninvasive brain-computer interface in humans, Proc. Natl. Acad. Sci. U. S. A. 101 (2004) 17849–17854.
[8] D.J. McFarland, W.A. Sarnacki, J.R. Wolpaw, Electroencephalographic (EEG) control of three-dimensional movement, J. Neural Eng. 7 (2010) 036007.
[9] B. Xia, O. Maysam, S. Veser, L. Cao, J. Li, J. Jia, H. Xie, N. Birbaumer, A combination strategy based brain-computer interface for two-dimensional movement control, J. Neural Eng. 12 (2015) 046021.
[10] J. Meng, S. Zhang, A. Bekyo, J. Olsoe, B. Baxter, B. He, Noninvasive electroencephalogram based control of a robotic arm for reach and grasp tasks, Sci. Rep. 6 (2016) 38565.
[11] A. Korik, R. Sosnik, N. Siddique, D. Coyle, Decoding imagined 3D hand movement trajectories from EEG: evidence to support the use of mu, beta, and low gamma oscillations, Front. Neurosci. 12 (2018).
[12] S. Crea, M. Nann, E. Trigili, F. Cordella, A. Baldoni, F.J. Badesa, J.M. Catalan, L. Zollo, N. Vitiello, N.G. Aracil, S.R. Soekadar, Feasibility and safety of shared EEG/EOG and vision-guided autonomous whole-arm exoskeleton control to perform activities of daily living, Sci. Rep. 8 (2018) 10823.
[13] Y. Chae, J. Jeong, S. Jo, Toward brain-actuated humanoid robots: asynchronous direct control using an EEG-based BCI, IEEE Trans. Robot. 28 (2012) 1131–1144.
[14] E. Tidoni, P. Gergondet, G. Fusco, A. Kheddar, S.M. Aglioti, The role of audio-visual feedback in a thought-based control of a humanoid robot: a BCI study in healthy and spinal cord injured people, IEEE Trans. Neural Syst. Rehabil. Eng. 25 (2017) 772–781.
[15] K. LaFleur, K. Cassady, A. Doud, K. Shades, E. Rogin, B. He, Quadcopter control in three-dimensional space using a noninvasive motor imagery-based brain-computer interface, J. Neural Eng. 10 (2013) 046003.
[16] B.H. Kim, M. Kim, S. Jo, Quadcopter flight control using a low-cost hybrid interface with EEG-based classification and eye tracking, Comput. Biol. Med. 51 (2014) 82–92.
[17] D. Shin, D. Shin, D. Shin, Development of emotion recognition interface using complex EEG/ECG bio-signal for interactive contents, Multimed. Tool. Appl. 76 (2017) 11449–11470.
[18] L. Bozhkov, P. Koprinkova-Hristova, P. Georgieva, Reservoir computing for emotion valence discrimination from EEG signals, Neurocomputing 231 (2017) 28–40.
[19] O. Al Zoubi, M. Awad, N.K. Kasabov, Anytime multipurpose emotion recognition from EEG data using a Liquid State Machine based framework, Artif. Intell. Med. 86 (2018) 1–8.
[20] A.K. Das, S. Suresh, N. Sundararajan, A discriminative subject-specific spatio-spectral filter selection approach for EEG based motor-imagery task classification, Expert Syst. Appl. 64 (2016) 375–384.
[21] E. Dong, C. Li, L. Li, S. Du, A.N. Belkacem, C. Chen, Classification of multi-class motor imagery with a novel hierarchical SVM algorithm for brain-computer interfaces, Med. Biol. Eng. Comput. 55 (2017) 1809–1818.
[22] E.A. Mohamed, M.Z. Yusoff, A.S. Malik, M.R. Bahloul, D.M. Adam, I.K. Adam, Comparison of EEG signal decomposition methods in classification of motor-imagery BCI, Multimed. Tool. Appl. 77 (2018) 21305–21327.
[23] K. Natarajan, U.R. Acharya, F. Alias, T. Tiboleng, S.K. Puthusserypady, Nonlinear analysis of EEG signals at different mental states, Biomed. Eng. Online 3 (2004) 7.
[24] J. Li, Y. Wang, L. Zhang, A. Cichocki, T.-P. Jung, Decoding EEG in cognitive tasks with time-frequency and connectivity masks, IEEE Trans. Cogn. Dev. Syst. 8 (2016) 298–308.
[25] A.L. Gardony, M.D. Eddy, T.T. Brunye, H.A. Taylor, Cognitive strategies in the mental rotation task revealed by EEG spectral power, Brain Cogn. 118 (2017) 1–18.
[26] J.C. Kao, S.D. Stavisky, D. Sussillo, P. Nuyujukian, K.V. Shenoy, Information systems opportunities in brain-machine interface decoders, Proc. IEEE 102 (2014) 666–682.
[27] B. He, B. Baxter, B.J. Edelman, C.C. Cline, W.W. Ye, Noninvasive brain-computer interfaces based on sensorimotor rhythms, Proc. IEEE (2015) 1–19.
[28] L.R. Quitadamo, F. Cavrini, L. Sbernini, F. Riillo, L. Bianchi, S. Seri, G. Saggio, Support vector machines to detect physiological patterns for EEG and EMG-based human-computer interaction: a review, J. Neural Eng. 14 (2017) 011001.
[29] D.R. Alonso, M.M.B.R. Vellasco, Spatial Filter Comparison for a Brain Computer Interface, Computational Intelligence (LA-CCI), IEEE Latin American Conference on, 2017, 2016.

[30] H. Jaeger, H. Haas, Harnessing nonlinearity: predicting chaotic systems and saving energy in wireless communication, Science 304 (2004) 78–80.
[31] S. Makeig, M. Westerfield, T.-P. Jung, J. Covington, J. Townsend, T.J. Sejnowski, E. Courchesne, Functionally independent components of the late positive event-related potential during visual spatial attention, J. Neurosci. 19 (1999) 2665–2680.
[32] T.-P. Jung, S. Makeig, C. Humphries, T.-W. Lee, M.J. McKeown, V. Iragui, T.J. Sejnowski, Removing electroencephalographic artifacts by blind source separation, Psychophysiology 37 (2000) 163–178.
[33] A. Mognon, J. Jovicich, L. Bruzzone, M. Buiatti, ADJUST: an automatic EEG artifact detector based on the joint use of spatial and temporal features, Psychophysiology 48 (2011) 229–240.
[34] S.L. Marple Jr., Digital Spectral Analysis with Applications, Prentice-Hall, Inc., Englewood Cliffs, NJ, 1987.
[35] D.J. McFarland, J.R. Wolpaw, Sensorimotor rhythm-based brain-computer interface (BCI): model order selection for autoregressive spectral analysis, J. Neural Eng. 5 (2008) 155–162.
[36] I. Farkas, R. Bosak, P. Gergel, Computational analysis of memory capacity in echo state networks, Neural Netw 83 (2016) 109–120.
[37] M.C. Ozturk, D. Xu, J.C. Principe, Analysis and design of echo state networks, Neural Comput. 19 (2007) 111–138.
[38] H. Cui, X. Liu, L. Li, The architecture of dynamic reservoir in the echo state network, Chaos 22 (2012) 033127.
[39] M. Inubushi, K. Yoshimura, Reservoir computing beyond memory-nonlinearity trade-off, Sci. Rep. 7 (2017) 10199.
[40] L. Bozhkov, P. Koprinkova-Hristova, P. Georgieva, Learning to decode human emotions with echo state networks, Neural Netw 78 (2016) 112–119.
[41] L. Sun, B. Jin, H. Yang, J. Tong, C. Liu, H. Xiong, Unsupervised EEG feature extraction based on echo state network, Inf. Sci. 475 (2019) 1–17.
[42] Z. Zhang, Z. Cheng, Z. Lin, C. Nie, T. Yang, A neural network model for the orbitofrontal cortex and task space acquisition during reinforcement learning, PLoS Comput. Biol. 14 (2018) e1005925.
[43] M. Venkatesh, J. Jaja, L. Pessoa, Brain dynamics and temporal trajectories during task and naturalistic processing, Neuroimage 186 (2019) 410–423.
[44] A. Prater, Spatiotemporal signal classification via principal components of reservoir states, Neural Netw 91 (2017) 66–75.
[45] Z. Gong, H. Chen, B. Yuan, X. Yao, Multiobjective learning in the model space for time series classification, IEEE Trans. Cybern. (2018) 1–15.
[46] S.E. Lacy, S.L. Smith, M.A. Lones, Using echo state networks for classification: a case study in Parkinson's disease diagnosis, Artif. Intell. Med. 86 (2018) 53–59.
[47] C. Yang, J. Qiao, H. Han, L. Wang, Design of polynomial echo state networks for time series prediction, Neurocomputing 290 (2018) 148–160.
[48] A. Dresden, The fourteenth western meeting of the American Mathematical Society, Bull. Am. Math. Soc. 26 (1920) 385–397.
[49] R. Penrose, A generalized inverse for matrices, Math. Proc. Camb. Philos. Soc. (1955) 51.